8. Detailed Design

8.1 Objective

Detail design is the next step in the development of the aircraft where individual components are designed. In this project a structural member in the aircraft's flap extension mechanism will be optimized for mass. The manufacturing constraint is that the component is to be laser cut from a $6.35mm$ thick Aluminium 6082-T6 plate. The structure has predefined holes through which it will be loaded and supported. The limit load for the component below which it cannot fail is 6kN and the ultimate load above which the structure will not be tested in 9kN. The efficiency of the structure will be measured using the merit index defined in Eq. 8.1.

$$\eta = \frac{LOAD}{MASS} \tag{8.1}$$

8.2 Parametric Optimization

The boundary conditions are similar to a beam simply supported at both ends. The deflection and maximum stress are thus closely dependent to the second moment of area. One way to achieve high bending stiffness and low weight is creating a pin-jointed structure where the trusses on the top will take the compressive loads and the bottom trusses will take tensile loads. The more they are spaced vertically from each other the higher their second moment of area will be but they also need to be connected at the support and loading holes which creates an optimization problem without a clear solution.

Idealization of component as a pin-jointed structure has a clear benefit of reducing the number of parameters of the problem. Given a topology of the structure its geometry can be fully specified using only the nodal positions and the heights of the individual trusses (the with is set to $6.35mm$). This significantly reduces the dimensionality of the optimization problem and allows to iterate over different possible designs much more quickly.

The structure is laser cut from a single piece of aluminium and therefore the trusses are rigidly connected and pin-jointed assumption about free rotation at nodes is not valid. The structure can be much more accurately modeled as a beam frame, this idealization is very computationally inexpensive to solve and thus also allows to iterate over many designs. The design iteration loop needs to be automated to take advantage of the number of iterations that can be done. Several optimization algorithms have be considered for this task such as simulated annealing or genetic algorithm but gradient descent was chosen for its implementation simplicity and reliability. Gradient descent can be used to find local minimum of some cost function by iterative computing the gradient of the cost function in respect to the parameters and updating the parameters as shown in Eq. 8.2. As the structure will be solved using a finite element solver it would be very complicated to compute the gradients analytically and therefore finite difference method will be used to approximate it. This requires a structure to be solved as many times as there are parameters in each iteration, this is not scalable to structured with many parameters, but for this application it is viable.

$$P_{opt}[i+1] = P_{opt}[i] - \frac{\delta Cost}{\delta P_{opt}} \cdot step \tag{8.2}$$

The gradient descent algorithm allow to find parameters that correspond to a local minimum of some cost function but that cost function needs to represent well the physical design goal. In this case the aim is to achieve the maximum merit index 8.1. The maximum load the structure is able to withstand should be between the limit and ultimate load because failing before the limit load is heavily penalized and any load the structure is supporting above the ultimate load is not counted. In this range it is hard to decide what is a good load to design for. A very constraining failure mode of the structure is the out of the plane buckling of the top spars under compression caused by the top

beam being significantly higher than wider. In structures designed for lower maximum load the height of the top beams is lower while the width is constant. This makes the structure proportionally thicker and thus more resilient to out of the plane buckling. On the other hand the manufacturing constraints dictate that the trusses must have minimal width of 3.5mm which might be inefficiently thick for a structure designed for low load. Further the holes are required to have a fixed amount of material around them and this will be a higher percentage of the total weight for a light structure. Lastly the real structure will have manufacturing and testing imperfections and will not behave exactly as in the simulation and so a healthy safety margin from the limit load should be designed for. This trade-off will be further explored quantitatively later.

Assuming that a designed maximum load is found the cost function should be defined such that the structure has minimum possible weight while all stresses are below the yield stress, buckling load is above the design load and maximum deflection is bellow the $5mm$ limit. Several versions of the cost function have been tried and the version which was found to most consistently converge to a desired solution is the shown in Eq. **??**-8.7 where $w_1, w_2 and w_3$ are tuned weights. The 8.4 is proportional to the surface area of the part calculated by multiplying and adding all the truss lengths and heights and will cause the weight optimization. The Costs 8.5,8.6 and 8.7 have similar form, their function is to ensure that the stresses, buckling loads and the deflection is below critical values. When the value of these variables is within the safe range the cost component and its gradient is zero and thus the optimization process is not affected. But when the critical value is crossed the second power ensures that the gradient of the cost function will gradually increase until it starts dominating the gradient descent vector and steers the parameters into a safe region. Because the critical value needs to be crossed in order for the correction to happen these values were selected slightly conservatively.

$$Cost = (Cost)_{Volume} + (Cost)_{stress} + (Cost)_{buckling} + (Cost)_{deflection} \tag{8.3}$$

$$(Cost)_{Volume} = \{L_{truss}\}^T \cdot \{h_{truss}\} \tag{8.4}$$

$$(Cost)_{stress} = (w_1 \cdot max(\sigma_{max} - \sigma_{yield}, 0))^2 \tag{8.5}$$

$$(Cost)_{buckling} = (w_2 \cdot max(LOAD_{buckling} - LOAD, 0))^2 \tag{8.6}$$

$$(Cost)_{deflection} = (w_3 \cdot max(v_{max} - v_{limit}, 0))^2 \tag{8.7}$$

8.3 Finite Element Solver

In order to implement the gradient descent algorithm a fast running beam frame solver is required where the structure can be defined and executed programmatically. As no such already existing solution was found it was decided that a custom solver will be developed in MATLAB. In order for the gradients to be computed the cost as a function of parameters needed to be continuous and differentiable. Only linear solver could thus be used as non-linear solver could introduce discontinuities. The solver needs to be able find the displacement and stresses in static loading case and the buckling load. The finite element method can compute these values by discrediting the structure into a linear beam elements connected at nodes. A stiffness matrix can be defined for each element that relates nodal deflections and loads as shown in Eq. 8.8. Two beam element formulations have be considered Euler-Bernoulli and Timoshenko. Timoshenko beam element is able to account for shear strain making it a very useful for beams with low slenderness ratio but suffers from shear locking when the slenderness ration is high. This can be mitigated by using reduced integration and fine mesh but for this application it was found that impractically many elements are required for solution to converge. Euler-Bernoulli element can accurately model beam behaviour even with very high slenderness ratio and only one element per truss is required for the static loading. It neglects the effects of shear strain but this was found to only result in very small error. The Euler-Bernoulli beam was thus selected to model the beam frame. The stiffness matrix of the entire structure can be found by superposing the transformed matrices of the individual elements. The boundary conditions can be applied to the structure by removing the degrees of freedom that are constraint. The two supporting holes are idealized as two nodes. The holes are tightly fitted with brass collars which restrain rotation about axes in the plane of the structure. The rotation about the axis normal to the plane is assumed to be free. Both Supports

further restrict the vertical and out of the plane deflection but only one support restrict the in plane horizontal movement as it is a rolling support. The node which is loaded is assumed to move freely. The load is applied through vector /b/ by setting the appropriate nodal degree of freedom to the value of the force. The nodal deflections can be found by solving the coupled linear system. The stresses are calculated in post-processing step using the shape functions by combining the bending and direct component.

$$[K]\{u\} = \{b\} \tag{8.8}$$

The buckling load of the structure can be found from the Eq. 8.9 where the $[K_\sigma]$ is the initial stress matrix and includes the beam direct stresses calculated in previous static loading step. The λ represents the multiplier of the initial load and the $\{u_{buckle}\}$ is shape of the buckling mode. A set of solutions to this problem can be found with eigenvalue analysis. The buckling critical load can be found using the smallest positive eigenvalue.

The material properties of the aluminium alloy were found using the CES software. It gives a range of values bot for the optimization mean values were used: $E = 72GPa$ and $\sigma_{yield} = 260GPa$. The results from the MATLAB solver with Euler-Bearnoulli elements and Abacus solver with shell elements is compared in Fig. 9.3 and 8.1. The results agree reasonable well and the MATLAB solver thus should be able to model trends in structural efficiency accurately. Further the MATLAB solver appears to be give higher deflections and lower buckling modes which means that the structure designed with this tool will be slightly conservative.

$$([K] + \lambda[K_\sigma]\{u_{buckle}\} = 0 \tag{8.9}$$

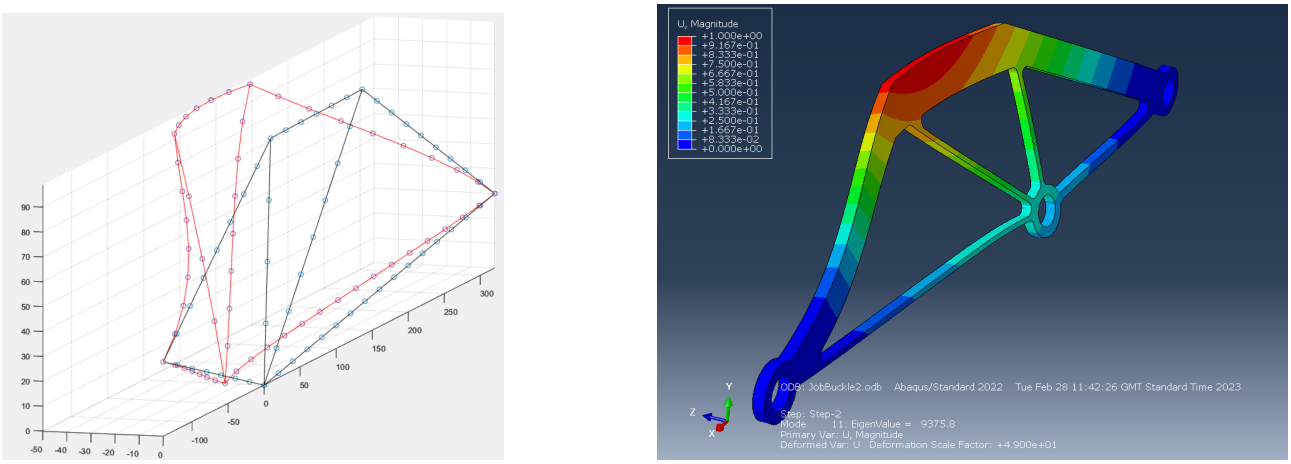

Figure 8.1: Figure 8.1 Comparison of the buckling modes computed with the MATLAB solver with Euler-Bernoulli assumption which yields buckling load of 8982N and the Abaqus solver with shell assumptions which yields buckling load of 9376N

8.4 Results of the parametric optimization

After the optimization loop with the gradient descent algorithm and beam frame solver was implemented it was found that the sensitivities to the nodal position (which change up to $200mm$) and the height of the trusses (which vary between $3.5mm$ and $20mm$) are widely different. A better results can be found if the optimization of nodal positions and heights are decoupled. In one optimization step the nodal positions are update only once while the heights of the trusses are updates up to 5 times. This helps with a problem where the nodal positions are updates too fast and the trusses height optimization can not keep up. An example of an evolution of the cost function during a optimization loop is shown in Fig. 9.4.

Now when the optimization algorithm is implemented the question whether it is more optimal to design for higher or lower loads is optimal. For the same topology two structures were optimized for the loads of $6kN$ and $9kN$ and their merit indexes were respectively $\eta = 37911$ and $\eta = 34995$. This experiment suggests that the higher design loads lead to higher merit indexes and even though this does not proof it for all scenarios it will be assumed that this trend is general. In order to ensure that the structure does not fail above the ultimate load $8kN$ was chosen as the design load.

The limitation of this optimization algorithm is that it can not automatically try different typologies and thus the truss connections and viable initial positions have to be manually specified. Several

simple typologies have been optimized for the design load and their converged surface area is compared in Figure 8.2. In general the converged designs tend to have a very thick top spars which have to resist the buckling and only very thin bottom spars under tension. Example of this can be seen in the Figure 8.1. Results show that structures where the extra nodes are added above the loading node perform much better than the opposite. Interesting is the example in right bottom corner which was given freedom to optimize a node both above and bellow the loading node. It converged to a geometry where the bottom node moved to the same point as the loading node and the structure thus effectively has no nodes below the loading node. The most efficient structure from the explored topologies is the one in the top right corner. It efficiently distributes the load onto the top spar using two points where the second one is not directly connected to the loading node but links to a bottom spar making it slightly shorter.

More complex design with more nodes and beams could reach even lower surface area but were not explored due to time constraints. It is probable than the benefit would be only very slight as the designs with many elements would be constrained by the minimum truss height limitation. Further in this model the weight of the fillets is not taken into account.

The parameters of the optimum design are shown in Table 8.1. As expected the top trusses under tension have much larger height and most of the weight of the structure can be attributed to the buckling constrain. An interesting observation is that the height of the top, middle beam (Element 5) is larger than the height of the two neighbouring beams (Elements 4 and 6). This can be explained by the profile of the buckling mode, the top beams deflect into shape resembling a harmonic period. This means that curvature is large in the middle and near the supporting nodes. During the optimization the stiffness of the middle spar was thus increased to combat the high curvature of the buckling mode. This effectively bring first and second mode closer together and increases the buckling load. The parametrization of the structure was such that the optimal height distribution could not be accurately represented. In order to improve this all top trusses were discritized into 5 elements as shown in Figure 9.7a. The nodal positions were fixed and the elements heights were further optimized. The resulting height distribution of the top trusses is shown in the Figure 9.7b. The trend resembles sinusoid as expected. This method yielded 2.3% surface area decrease which is a non-negligable improvement but it has also negatives. It was found that the buckling load is more sensitive to changes in the top truss height distribution than when the trusses had uniform height. It can be expected that the structure with optimized height distribution will also be more sensitive to manufacturing and testing imperfections. Without the ability to accurately test both parts with imperfections it was decided that a safer choice is to use the structure with constant truss height. But this method appears to be a promising way how the part could be further optimized in future.

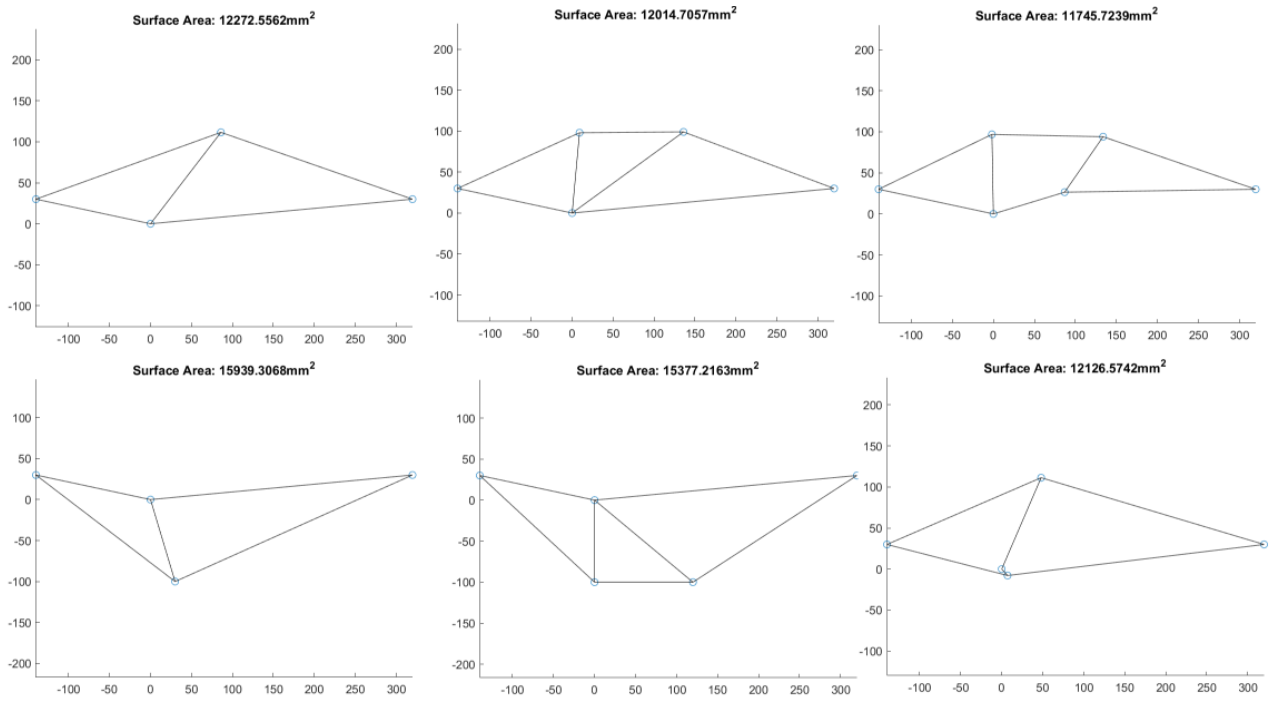

Figure 8.2: Comparison between the calculated surface area of different structures

Table 8.1: The list of nodes and beam elements

Node	x (mm)	y (mm)
1	0	0
2	-140	30
3	320	30
4	86.75292	26.2286
5	-1.60288	96.97379
6	134.4319	94.41006

Element	Node 1	Node 2	height (mm)
1	1	2	5.277495
2	1	4	5.318469
3	4	3	4.145542
4	2	5	17.87935
5	5	6	22.21357
6	6	3	16.27997
7	1	5	3.5
8	4	6	3.5

8.5 CAD

the approximate geometry of the structure was optimized but in order to manufacture it a CAD model needs to be created that includes all the manufacturing constraints. The CAD was created in SOLIDWORKS software by first sketching the wire-frame of the idealized structure and than adding the top and bottom edge of each truss using the offset tool. The support and loading holes were added and all extra lines were removed using the trim tool. At the nodes the edges were smoothly connected using a $4mm$ radius fillet for the internal corners and $10mm$ radius fillet for external corners. The sketch was than extruded to the appropriate thickness to create the 3D model of the part. The drawing of the final structure is shown in Fig. 8.3. The weight of structure was estimated using assuming the material density of $2.7g/cm^3$ to be $212g$.

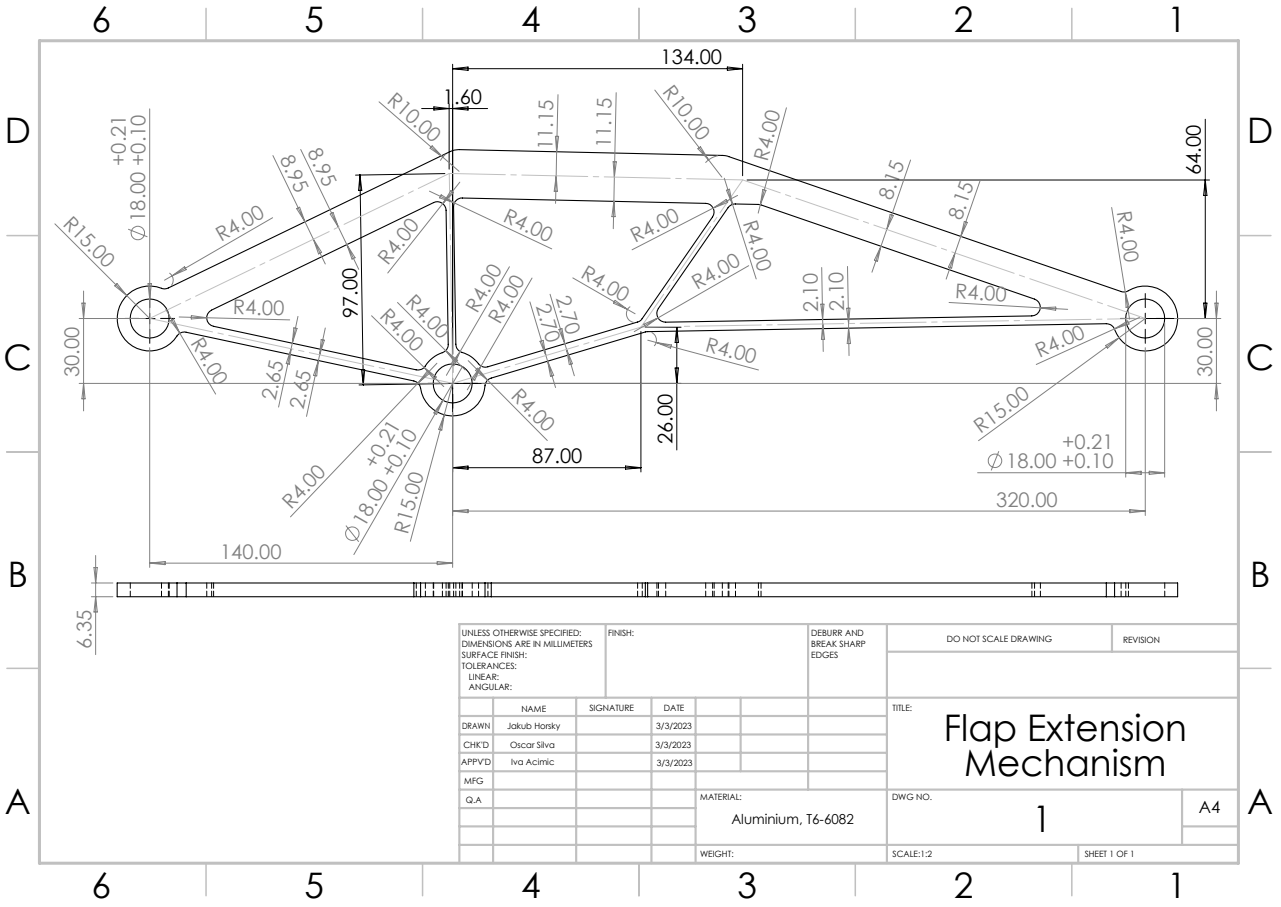

Figure 8.3: Engineering drawing of the detailed part

8.6 Design Evaluation

The structure was optimized under the modeling assumption of Euler Beam Elements. This neglects physical effects such as shear and transverse strain and geometry at the nodes such as fillets or the rings around the loading and supporting holes. Much more accurate prediction can be made by using Finite Element Analysis with 3D elements where the entire geometry of the structure is considered. For

this task the commercial FEA software Abaqus was used. The geometry of the part was import and meshed using 3D stress 8-node linear elements with Medial axis algorithm which created structured mesh along the beams. The material was defined with the same constants as in the MATLAB solver. The boundary conditions were applied using a Multi Point Constraint (MPC) which helps to model the interaction between the support collar and the hole. MPC creates a rigid connection between the internal surface of the whole and a reference point in the centre of the hole. The same boundary condition as in the beam frame model were than applied on the reference points which allow the hole to freely rotate around the out of the plane axis. The load was similarly applied thought a MPC inside the loading hole. The structure was loaded in linear static step with $8kN$ and in buckling linear perturbation with the reference value of $1N$.

An important step in validating a FEA is showing that the result is mesh independent. This can be done by computing some value of interest for different element size and seeing for what mesh size the result converges. Such study was conducted with maximum vertical deflection and Von Mises stress in the static loading step and with critical buckling load and results are plotted against the number of elements in Fig. 8.4a. It shows that static step results converge much faster than the buckling step results. This can be explained by the fact that static loading is essentially 2 dimensional and thus does not require many elements through the thicness of the structure. On the other hand the buckling analysis requires the modeling of variations thought the thickness.

The solved Von Mises stresses under $8kN$ loading is shown in Fig. 9.6a. The maximum stress is $260.8MPa$ which is remarkably close the the limit of $260MPa$ enforced in the optimization. It is slightly larger than the estimated yield stress but this is not a problem because the structure will be able to withstand even higher stresses with plastic deformation. The results of the buckling analysis is shown in the Fig. 9.6b and the critical buckling is $8447N$ which is higher than what was predicted by the beam frame solver. Because the estimated material yield stress was reached during the linear static loading analysis more accurate estimate of the structural behaviour was computed using non-linear static loading analysis where the stress-strain curve of the material was specified. The the structure was loaded using imposed displacement of $5mm$ and the resulting stress is shown in Fig. 9.5b. The max Von Mises stress is still well below the tensile strength of $295MPa - 344MPa$ according to CES software. The loading hole deflection is plotted against the applied load in Fig. 9.5a and it shows that the $5mm$ vertical deflection limit is not reached even when the ultimate load is applied. This will likely not make any difference as the structure is expected to buckle before the ultimate load is reached.

The design of the structure can thus be expected to withstand the design load of $8kN$ and likely will able to go above that before the expected buckling failure.

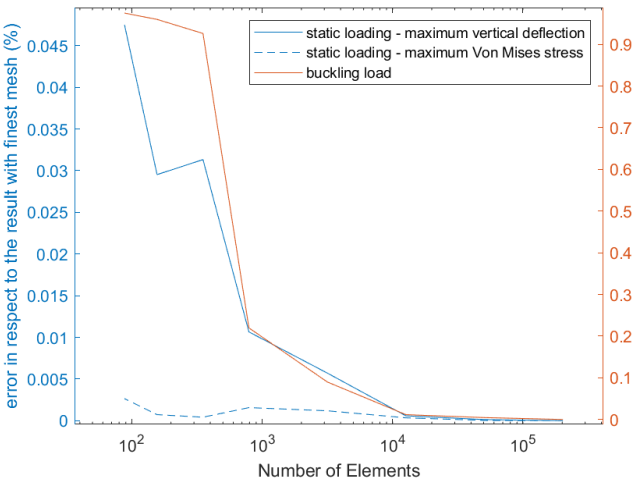

Figure 8.4a: Mesh convergence study of the FEA of the linear static and buckling step. The compared values are presented in the form of percentage error in respect to value computed with the finest mesh

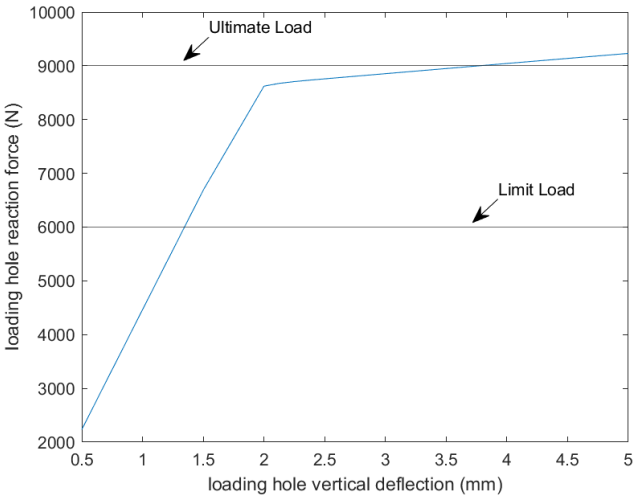

Figure 8.4b: The relationship between the applied load and the vertical deflection of the loading hole obtained using non-linear static FEA

C Detail Design

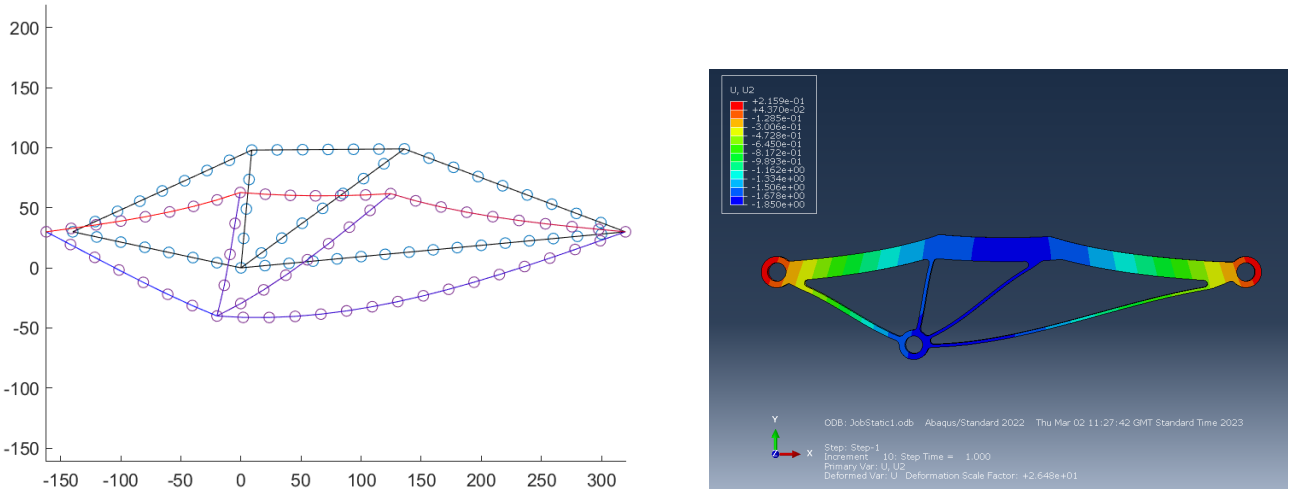

Figure 9.3: Figure 8.1 Comparison of the deflections under static loading computed with the MATLAB solver with Euler-Bernoulli assumption which yields max vertical deflection of -1.98mm and the Abaqus solver with shell assumptions which yields buckling load of $-1.85mm$

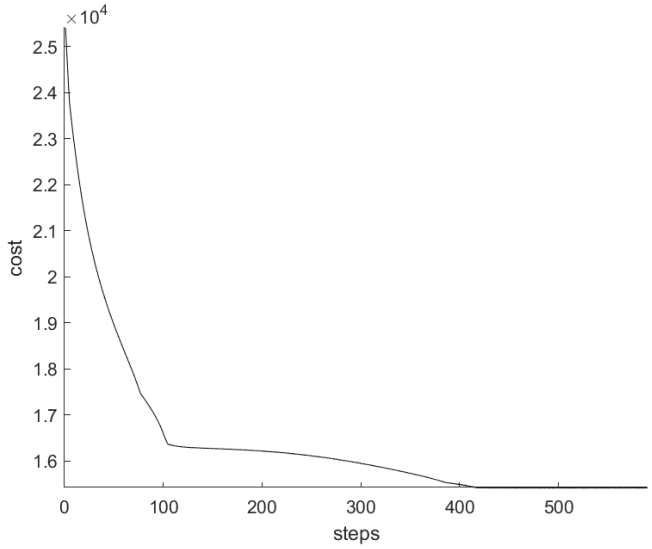

Figure 9.4: Example of a change in cost function during optimization loop

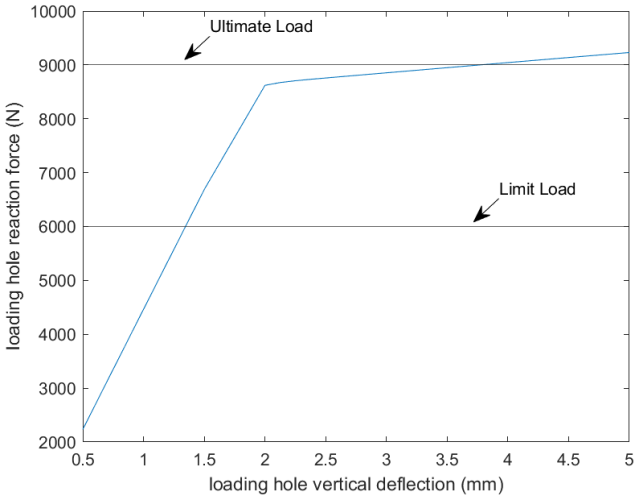

Figure 9.5a: Plot of the vertical deflection of the loading hole against the applied load computed with non-linear static loading step

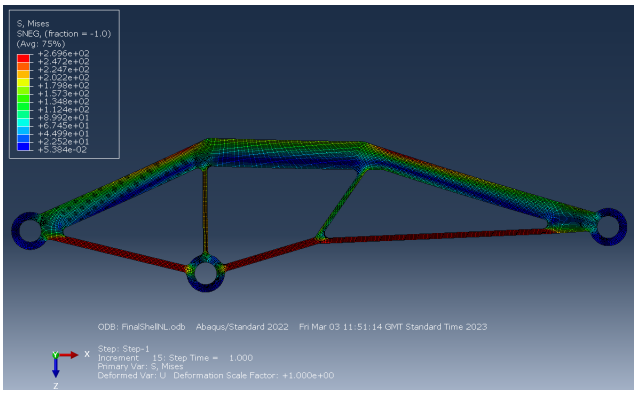

Figure 9.5b: Von Mises stress in the structure after $5mm$ of vertical displacement was applied on the loading hole. The results were obtained using non-linear static solver

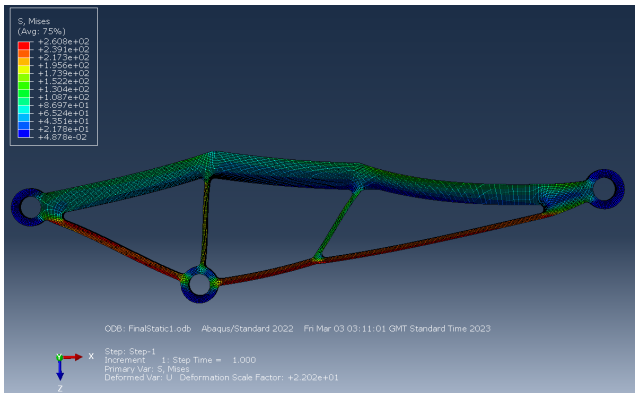

Figure 9.6a: Von Misen stress in the structure under $8kN$ loading solved with linear solver

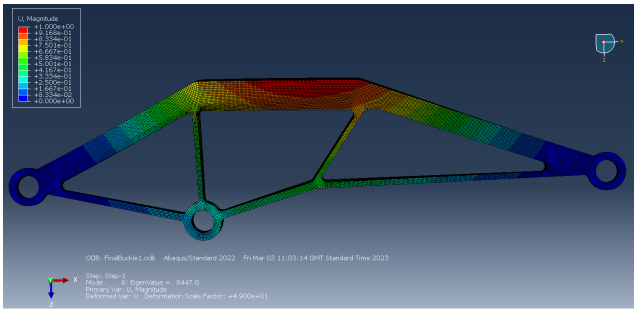

Figure 9.6b: Critical buckling mode of the structure with the buckling load of $8447N$

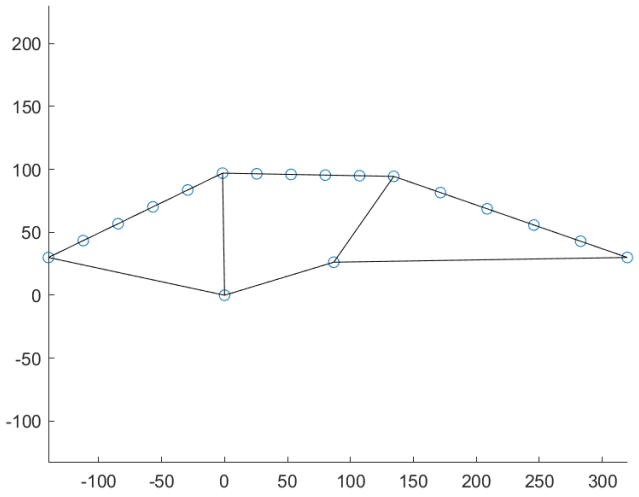

Figure 9.7a: Discretization of the top truss

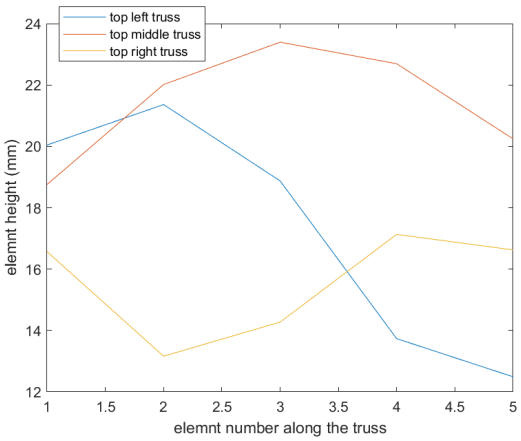

Figure 9.7b: Optimized height distribution of the top spars